

Rapid formation of porphyry copper deposits evidenced by diffusion of oxygen and titanium in quartz

Federico Cernuschi^{1*}, John H. Dilles¹, Stephanie B. Grocke², John W. Valley³, Kouki Kitajima³, and Frank J. Tepley III¹

¹College of Earth, Ocean, and Atmospheric Sciences, Oregon State University, Corvallis, Oregon 97331-5506, USA

²Department of Mineral Sciences, National Museum of Natural History, Smithsonian Institution, Washington DC, 20560, USA

³Department of Geoscience, University of Wisconsin–Madison, Madison, Wisconsin 53706, USA

ABSTRACT

The lifespan of magmatic-hydrothermal activity that results in large and economically viable porphyry copper deposits remains poorly described. Here, we estimate the duration of the magmatic-hydrothermal fluid flow at 700 °C to <350 °C using diffusion profiles of Ti and δ¹⁸O in quartz from Fe, Cu, and Mo sulfide-bearing hydrothermal veins and porphyry dikes at the Haqira East porphyry copper deposit, Peru. *In situ* measurements indicate all vein quartz is zoned in Ti (1–120 ppm), whereas high-temperature quartz has been re-equilibrated at 450 °C to δ¹⁸O = 10.7‰. We use diffusion modeling to reproduce the observed Ti and δ¹⁸O profiles, which provides lifespan estimates at Haqira of 75–170 k.y. for the period from initial magma and fluid injection at 700 °C to cooling below 350 °C. The bulk of the Cu-Mo-Au ore formed in ≤35 k.y., indicating that large-scale, economic porphyry copper deposits can form rapidly.

INTRODUCTION

Porphyry copper deposits are major Cu-Mo-Au producers, genetically related to shallowly emplaced arc-type granitoids (see the GSA Data Repository¹; Seedorff et al., 2005). Magmatic-hydrothermal fluids separate from magma and ascend by hydrofracturing the overlying wall-rock where they depressurize, cool from ~700 °C to <350 °C, and react with rock to form quartz veins and both vein-hosted and disseminated Fe, Cu, Mo, and Au-bearing sulfides. Significant Cu-ore resources require the emplacement and release of large volumes of fluid from a single magmatic intrusion (e.g., 4 Mt of Cu require >2 Gt of fluid; see the Data Repository). It remains unclear how rapidly this process occurs. U-Pb zircon ages of porphyry intrusions and Re-Os ages of hydrothermal molybdenite suggest fluid flow durations of ≤100 k.y. for the entire ore-formation process at Bingham (Utah, USA) and Bajo de la Alumbrera (Argentina; von Quadt et al., 2011), and for each of the several individual mineralizing fluid pulses at El Teniente (Chile; Spencer et al., 2015). Modeling of the widths and taper of alteration selvages yields shorter durations: ~100 yr for individual veins formed during sericitic alteration at Butte (Montana, USA; Geiger et al., 2002), and ~20 yr and ~900 yr for K-silicate alteration at Bajo de la Alumbrera and Butte, respectively (Cathles and Shannon, 2007). At Butte, diffusion

modeling of Ti-in-quartz gradients in growth zones imaged by scanning electron microscope cathodoluminescence (SEM-CL) suggest porphyry magma residence times of 1 k.y., and formation and cooling of various generations of hydrothermal vein quartz in 10 yr to 10 k.y. (Mercer et al., 2015).

We estimate the hydrothermal lifespan of the Haqira East porphyry Cu-Mo deposit (Peru) using SEM-CL images of quartz from porphyry dikes and veins, and *in situ* Ti and δ¹⁸O compositions. Assuming Ti and δ¹⁸O compositional gradients were initially abrupt step-like changes, we model the time to produce the gradients using experimental diffusivities, estimated temperatures, and cooling rates. The gradients of δ¹⁸O in quartz analyzed by ion microprobe (SIMS) provide a novel approach to quantify time scales at low temperature (<400 °C) because oxygen isotope diffusivity is ~10,000 times faster than Ti diffusivity in quartz.

ORE GEOLOGY

Haqira East is a relatively deeply emplaced porphyry Cu-Mo-Au deposit (>8 km; see the Data Repository). It is hosted in a ca. 34 Ma subvertical granodiorite stock cut by a series of granodiorite porphyry dikes that are part of the Andahuaylas-Yauri batholith of southern Peru. Hydrothermal veins were emplaced in a regular sequence based on cross-cutting relationships (Fig. 1A; Cernuschi et al., 2013). We refer to various vein types using common conventions, as defined by Seedorff et al. (2005). Early aplite dikes are cut by sinuous and milky deep quartz veins (DQ) with traces of Cu-sulfides that are synchronous with porphyry dike emplacement.

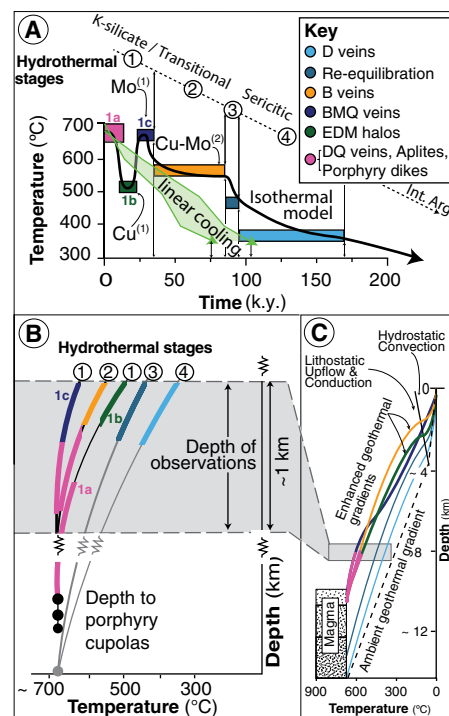


Figure 1. Summary of estimated time scales of the Haqira East porphyry Cu-Mo-Au deposit (Peru). A: Temperature and time evolution of the four hydrothermal stages and the formation of the Cu-Mo-ore. **B,C:** Schematic depth section illustrating the evolution of the geothermal gradient resulting from porphyry intrusions and fluid ascent. BMQ—banded molybdenite-quartz; EDM—early dark micaceous; DQ—deep quartz; Int.Arg.—intermediate argillic.

Younger EDM (early dark micaceous) alteration selvages contain biotite–muscovite–K-feldspar–bornite–chalcopyrite ± quartz. EDM selvages on fractures that rarely have quartz vein fill produce high-grade Cu ore, and are cut by banded molybdenite–quartz veins (BMQ) that introduce most of the Mo to the deposit. BMQ veins are cut by quartz veins that have a centerline infilled with bornite–chalcopyrite ± molybdenite and contribute Cu and Mo to ore (B veins). Quartz–muscovite–pyrite ± rare chalcopyrite veins with muscovite ± quartz ± pyrite alteration selvages cut all the earlier veins (D veins). Four Re/Os isotopic ages of molybdenite from BMQ veins

*E-mail: fede@eclectic-rock.com

¹GSA Data Repository item 2018209, Ti and δ¹⁸O in quartz data, diffusivity calculations and diffusion models, is available online at <http://www.geosociety.org/datarepository/2018/> or on request from editing@geosociety.org.

average 33.75 ± 0.15 Ma, and one $^{40}\text{Ar}/^{39}\text{Ar}$ age of muscovite from a D vein yields 33.18 ± 0.21 Ma; these data provide a maximum lifespan of the Haquira hydrothermal system of ~ 600 k.y. (Cernuschi et al., 2013).

METHODS

Quartz in five polished sections was imaged using a FEI Quanta 600 field emission gun (FEG) scanning electron microscope (SEM) equipped with a Gatan MiniCL cathodoluminescence grayscale detector at Oregon State University (OSU, Corvallis, Oregon, USA; see the Data Repository for extended methods). The Ti content of quartz was measured using a CAMECA SX-100 electron microprobe (EMP; Table DR2 in the Data Repository) or by laser ablation–inductively coupled plasma–mass spectrometry (LA-ICP-MS; Table DR3) at OSU with detection limits of 13 and 0.2 ppm, respectively. CL grayscale images were processed with National Institutes of Health ImageJ software (<https://imagej.nih.gov/ij/index.html>) along line traverses, and calibrated using spot analyses of Ti. The $\delta^{18}\text{O}$ of quartz was analyzed *in situ* from 10- μm -diameter spots using a CAMECA IMS-1280 ion microprobe (SIMS) at the University of Wisconsin (Madison, Wisconsin, USA). Values are reported in per mil (‰) relative to Vienna Standard Mean Ocean Water (V-SMOW) with spot-to-spot precision of $<0.3\%$ (Tables DR4–DR9).

RESULTS

Five quartz samples (Table DR1; Figs. DR1 and DR2) selected based on vein cross-cutting relationships are representative of four progressively cooler thermal stages from early mineralization to post mineralization (Fig. 1A): a quartz phenocryst from a porphyry dike (Fig. 2); an EDM selvage re-opened by a B vein that is, in turn, cross-cut by late quartz in fractures (Fig. 3); a B vein rimmed by late quartz (Fig. 4); and two D veins (Fig. 5; Figs. DR3 and DR4).

The quartz phenocryst (Fig. 2) is CL-zoned, from core to rim, from light to dark gray (24–54 ppm Ti), and contains one internal band of bright CL and a second 10- μm -thick rim with ~ 75 ppm Ti. The bright CL of the phenocryst rim is similar to quartz in the adjacent aplitic porphyry groundmass (Fig. 1), and to hydrothermal quartz in DQ and BMQ veins.

The chalcopyrite-bornite-bearing EDM selvage envelopes a vein of mosaic-textured, uniformly gray-CL quartz with 24–47 ppm Ti that is crosscut by a B vein composed of strongly CL-banded quartz growth zones infilled by slightly later bornite-chalcopyrite (Fig. 3). B vein quartz is generally euhedral, with alternating gray-CL and bright-CL growth bands that range from 31 to 53 ppm Ti and from 69 to 84 ppm Ti, respectively. The $\delta^{18}\text{O}$ of quartz in gray-CL and bright-CL from all EDM and B

vein bands is indistinguishable (mean of $10.67 \pm 0.36\%$; Fig. 3C).

Euhedral quartz from a different B vein sample (Fig. 4) also displays bright-CL (92–114 ppm Ti) and gray-CL (39–59 ppm Ti) growth bands with indistinguishable $\delta^{18}\text{O}$ compositions (mean of $10.40 \pm 0.44\%$; Fig. 4C). B vein quartz is fractured, partially dissolved, and then overgrown by rims and fracture-fillings of dark-CL quartz (<13 ppm Ti, below EMP detection limit; Fig. 4A). Dark-CL quartz has higher $\delta^{18}\text{O}$ compositions (mean of $12.49 \pm 0.94\%$; Fig. 4C) than B vein quartz.

A late D vein (Fig. 5) contains weakly growth-zoned, medium gray-CL quartz with 13–25 ppm Ti that is locally overgrown by dark-CL quartz with 1–6 ppm Ti (LA-ICP-MS). In D veins, the $\delta^{18}\text{O}$ of medium-gray CL quartz ranges from 9.7% to 12.6% (mean of $11.16 \pm 1.45\%$), and the dark-CL quartz ranges from 10.8% to 14.4% (mean of $12.57 \pm 1.82\%$). The medium gray-CL and dark-CL D vein quartz is similar in CL and isotopic composition to late quartz that fills fractures (Fig. 3B) and rims quartz in all early veins (DQ through B; Fig. 4B). Two spot analyses within fracture-filling quartz in an EDM vein yield $\delta^{18}\text{O}$ of 12.4% and 11.3% (Fig. 3C) and four additional spot analyses within a B vein range from 11.05% to 13.14% (Table DR4).

In summary, all quartz contain Ti diffusion profiles documented by variable CL intensity and correspondingly varied Ti contents of

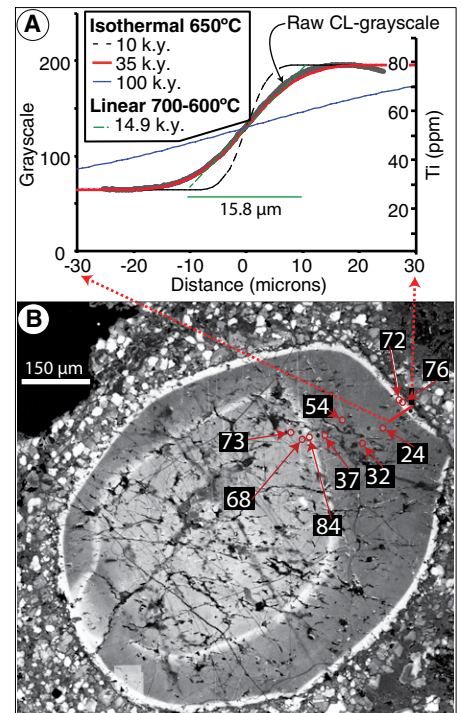


Figure 2. Scanning electron microscope cathodoluminescence (SEM-CL) image of a zoned quartz phenocryst in a porphyry dike composed of a light gray-CL inner core and a gray-CL outer core separated by a thin bright-CL band. A narrow bright-CL, high-Ti quartz band rims the gray-CL, lower-Ti outer core (B). A diffusion model calculated at $\sim 650^\circ\text{C}$ for Ti gradients at the core-rim boundary indicates a maximum time scale of 35 k.y.

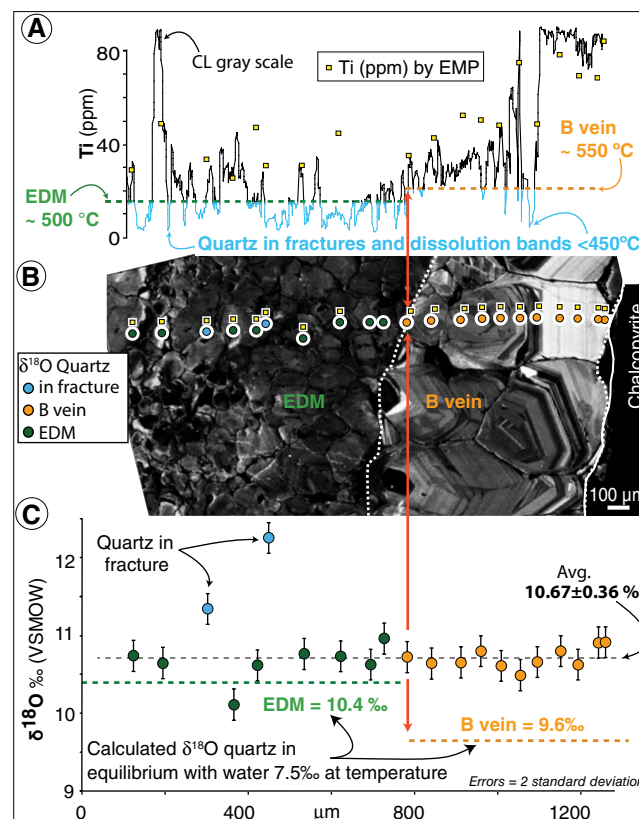


Figure 3. A: Ti-in-quartz data (electron microprobe, EMP) and cathodoluminescence (CL) grayscale profile along transect shown in B. TitaniQ temperature of EDM (early dark micaceous) and B vein quartz was calculated from the mean of the lowest Ti zones. **B:** SEM-CL of EDM gray-CL mosaic quartz re-opened and overgrown by gray- to bright-CL banded B vein euhedral quartz. **C:** Measured $\delta^{18}\text{O}$ ‰ (secondary ion mass spectrometry, SIMS) of quartz along the transect and calculated $\delta^{18}\text{O}$ ‰ based on the estimated temperature of precipitation (Table DR6 [see footnote 1]). VSMOW—Vienna Standard Mean Ocean Water.

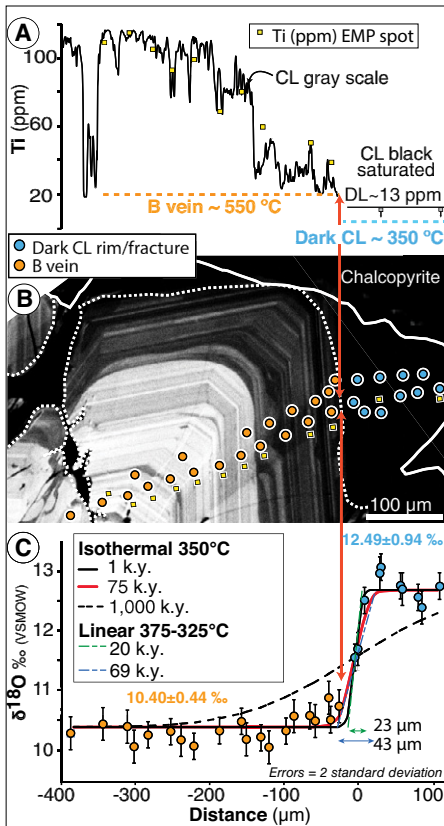


Figure 4. A: Ti-in-quartz data (electron microprobe, EMP) and cathodoluminescence (CL) grayscale profile along transect shown in **B**. Precipitation temperatures were calculated using the TitaniQ geothermometer of the lowest Ti zones. **B:** SEM-CL image of quartz illustrating inner, gray-CL zoned euhedral B vein quartz bands, two or more dissolution surfaces, and an overgrowth rim of later lower-temperature dark-CL quartz. **C:** $\delta^{18}\text{O}$ ‰ of quartz (secondary ion mass spectrometry, SIMS) along transect. B vein quartz varies from 10.1‰ to 10.7‰ whereas the dark-CL rim is ~12.7‰. The diffusion model for the observed $\delta^{18}\text{O}$ gradient between the B vein gray-CL quartz (10.1–10.7‰) and dark-CL rim (~12.7‰) suggests formation in ≤ 75 k.y. at ~350 °C. VSMOW—Vienna Standard Mean Ocean Water.

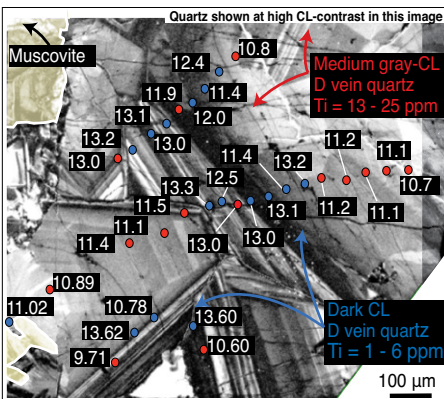


Figure 5. High-contrast scanning electron microscope cathodoluminescence (SEM-CL) image of quartz-muscovite-pyrite D vein. Quartz is euhedral and composed of bands of medium gray-CL (higher Ti, $10.8 < \delta^{18}\text{O} < 13.6\text{‰}$) and dark-CL (lower Ti, $9.7 < \delta^{18}\text{O} < 12.6\text{‰}$).

spot analyses. Early quartz in the EDM and B veins have relatively low and homogeneous $\delta^{18}\text{O}$ compositions of ~10.6‰. In contrast, the medium-gray and dark-CL quartz in the later D veins and fractures have relatively high $\delta^{18}\text{O}$ compositions of ~11.2 and 12.5, respectively.

DISCUSSION

Formation Temperature

Formation temperatures were estimated by the TitaniQ geothermometry of Huang and Audétat (2012). The observed bright-CL and high-Ti quartz is interpreted to result from enhanced incorporation of Ti in crystal defects during non-equilibrium rapid quartz growth triggered by magmatic degassing during ascent. High growth rates of quartz yield spuriously high formation temperatures, by up to 100 °C (Huang and Audétat, 2012); therefore, we use the lowest Ti contents of quartz to estimate temperature.

Assuming crystallization in a magma chamber below the ore zone at ~300 MPa, the gray-CL outer part of the igneous quartz phenocryst (24–54 ppm Ti; Fig. 2) yields a TitaniQ temperature of 650–703 °C. Fluid inclusions in all veins are liquid + vapor, indicating trapping pressures >140 MPa at near-lithostatic conditions (see the Data Repository). Using 140 MPa pressure and the lowest Ti contents of quartz, EDM veins (27–49 ppm Ti) and B veins (18–59 ppm Ti) yield TitaniQ temperatures of 566–621 °C and 543–640 °C, respectively. D veins likely formed at near-hydrostatic pressure (~110 MPa), in which case medium-gray CL quartz (13–25 ppm Ti) and dark-CL quartz (1–6 ppm Ti) have TitaniQ temperatures of 494–546 °C and 343–441 °C, respectively. We consider all estimates maxima because of the Ti-in-quartz growth rate issue, and use conservatively low temperatures for isothermal diffusion models consistent with selvage mineral phase equilibria (i.e., 650 °C for magmatic quartz, 500 °C for EDM veins, 550 °C for B veins, and 450 to 350 °C for D veins; Seedorff et al., 2005; Table DR5).

Diffusion Models

We modeled isothermal diffusion in four quartz samples to calculate the lifespan of four thermal stages (650 °C, 550 °C, 450 °C and 350 °C) that represent the cooling of the magmatic-hydrothermal fluid from K-silicate to sericitic alteration (Fig. 1A). For each quartz type, we used the minimum estimated temperature to model the maximum time scale (Table DR5). The preferred models were selected using the best χ -squared goodness-of-fit statistic, which was also used to estimate the error for each model (see the Data Repository, Table DR6, Figs. DR5–DR7, DR10, and DR11). We used the equation from Crank (1975) for one-dimensional diffusion, and the spherical diffusion equation for closely spaced fractures in quartz

(see the Data Repository). We also modeled the same diffusion profiles using the constraint of cooling from 700 to 325 °C (Watson and Cherniak, 2015, Table DR7).

Time Scales

Stage 1: Magmatic and Main Cu-Mo Stage

The Ti-in-quartz gradient between the quartz phenocryst core and its rim (Fig. 2A) is interpreted to have formed during rapid porphyry emplacement, and therefore represents the earliest and highest-temperature stage of the magmatic-hydrothermal system (Fig. 1A). Porphyry dikes were sequentially cut by aplites, and DQ and BMQ veins that all contain similar bright-CL quartz formed at a temperature of ~650 °C. The Cu-rich EDM selvages have ages intermediate between DQ and BMQ veins and formed at a lower temperature of ~500 °C, which suggest at least one cycle of cooling followed by heating (Fig. 1A). A diffusion model calculated at ~650 °C for Ti gradients at the core-rim boundary of a porphyry quartz phenocryst indicates a maximum time scale of 35 k.y. (± 15 k.y.) for the porphyry to BMQ stage; linear cooling from 700 to 600 °C yields 14.9 k.y. (Fig. 2A; Figs. DR6 and DR7).

Stage 2: Second Cu-Mo Stage

B veins with Cu-Mo sulfides contain bright-CL and gray-CL growth-banded quartz with resorption surfaces that attest of several temperature/pressure fluctuations (Figs. 3B and 4B). Using a mean temperature of 550 °C, diffusion models for three B vein Ti gradients provide a maximum time scale of ~50 k.y. (+50/–30 k.y.); linear cooling from 600 to 475 °C yields 25.4 to 40.9 k.y. (Fig. 1; Figs. DR6 and DR7).

Stage 3: 450 °C $\delta^{18}\text{O}$ Homogenization of Early High-Temperature Quartz

We assume that magma-derived hydrothermal fluids had relatively uniform $\delta^{18}\text{O}$, and produced all veins types (cf. Reed et al., 2013). We calculate a $\delta^{18}\text{O}$ composition of parent magmatic-hydrothermal water of 7.5–8.0‰ based on observed quartz compositions (Table DR6), application of quartz-water fractionation factors at hydrothermal conditions (Zhang et al., 1989), and our estimated vein formation temperatures (Table DR8). Our calculations suggest that the earlier medium gray-CL quartz ($\delta^{18}\text{O}$ of ~11.2‰) and later dark-CL quartz ($\delta^{18}\text{O}$ of ~12.5‰) from D veins are in equilibrium with magmatic water ($\delta^{18}\text{O} = 7.5\text{‰}$; Taylor, 1968) at 450 and 380 °C, respectively. These temperatures are in good agreement with independent estimates derived from phase equilibria and the TitaniQ geothermometer. In contrast, the quartz in both EDM and B veins have identical mean $\delta^{18}\text{O}$ values (~10.6‰) that are in equilibrium with 7.5‰ water at ~475 °C, a slightly lower

temperature compared to estimates from phase equilibria and TitaniQ geothermometry (500–550 °C). We interpret that oxygen within EDM and B vein quartz diffusively homogenized at ~450 °C with magmatic water that penetrated along fractures, that likely result from contraction upon cooling and are infilled locally by later medium gray-CL quartz (Fig. 3A; Figs. DR8 and DR9). Nonetheless, Ti contents of high-temperature EDM and B vein quartz attest to little reequilibration at <450 °C because of the low Ti diffusivity (Fig. 3). We modeled spherical three-dimensional (3-D) oxygen diffusion, along the 3-D network of fractures and dissolution bands that are commonly spaced every 40–120 μm (20–60 μm radius, respectively; Fig. DR9). Time scales were calculated for δ¹⁸O profiles at 450 °C for diffusion between a 7.5‰ magmatic water and B vein quartz that was originally 9.6‰ (Fig. 6). Spherical diffusion models yield time scales of 1 and 10 k.y. (+10/–4 k.y.) to re-equilibrate across a distance of 20 and 60 μm, respectively. We consider the latter as the maximum duration of this stage (Fig. 1).

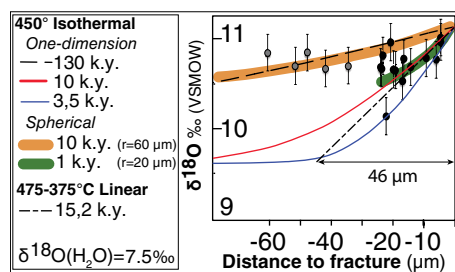


Figure 6. Quartz δ¹⁸O ‰ (secondary ion mass spectrometry, SIMS) versus measured distance to fracture or dissolution band in a B vein (Fig. 2). Analyzed spots located at <20 μm and 30–60 μm from fracture/dissolution bands are black and gray, respectively. Spherical diffusion models yield 1 k.y. and 10 k.y. to re-homogenize quartz at <20 μm and <60 μm from fractures, respectively. VSMOW—Vienna Standard Mean Ocean Water; r—radius.

Stage 4: Late Quartz in D Veins and Fractures

The fractures through early quartz that remained opened were later filled during cooling by dark-CL quartz. One dark-CL D vein contains quartz with 1–6 ppm Ti formed at ~350 °C (Fig. 5), a temperature also assumed to characterize the dark-CL quartz in microfractures (Fig. 3). Modeling the δ¹⁸O diffusion profile of a late 12.7‰ dark-CL rim on earlier 10.7‰ B vein quartz gives a maximum time of 75 k.y. (+25/–15 k.y.) at 350 °C and 69 k.y. for linear cooling from 375 to 325 °C (Figs. 1 and 4B).

CONCLUSIONS

The lifespan of the magmatic-hydrothermal system of deeply emplaced (>5 km depth) porphyry copper deposits can be relatively short. The isothermal diffusion modeling presented here uses conservatively low temperature estimates that provide a maximum magmatic-hydrothermal lifespan of 170 k.y. (+100/–64 k.y.) for cooling from 650 to 350 °C across four thermal stages (Fig. 1A). The corresponding linear cooling from 700 to 325 °C provides even shorter estimates of 75–153 k.y. (Fig. 1A). Significant ore resources can form even more rapidly. At Haqira East, the bulk of the 4.2 Mt of Cu, 37,000 t of Mo, and 28 t of Au contained in the ore were formed during stage 1 in ≤35 k.y. (Fig. 1A), implying that >2 Gt of fluid was released in this same period.

During the ore-forming processes of stages 1 and 2, magmatic-hydrothermal fluids ascended, heated the wall rock, and effectively produced an enhanced geothermal gradient and K-silicate to transitional alteration (Figs. 1B and 1C). Stage 1 includes the initial DQ veins and aplites at ~650 °C, later Cu-rich EDM veins at ~500 °C, and then a thermal reversal to form Mo-rich BMQ veins at ~650 °C. Additional Cu-Mo ore, hosted in B veins, was formed during stage 2 in ≤50 k.y. upon cooling to 550 °C.

The post-ore-formation cooling history is included in stages 3 and 4, reflecting the degradation of the geothermal gradient, as a response to crystallization of the deep magma chamber source of porphyry dikes and the decline of the magmatic-hydrothermal fluid flux. In stage 3, the δ¹⁸O of preexisting quartz was partially homogenized in ≤10 k.y. at ~450 °C and in stage 4, sericitic alteration occurred at ~350 °C in a period of ≤75 k.y. The latter duration likely includes regional slow cooling attending the deep emplacement of Haqira. We expect significantly shorter time scales for shallowly emplaced porphyry deposits (<5 km depth) that cool faster.

ACKNOWLEDGMENTS

We thank First Quantum Minerals Ltd. (Vancouver, Canada) and the U.S. National Science Foundation (NSF; grants EAR-1355590, EAR-1658823, EAR-1524336 and EAR-1447730) for making this research possible. We are indebted to Brendan Murphy, Chris Clark, David Cooke, Celestine Mercer, Daniele Cherniak, and one anonymous reviewer for their insightful reviews.

REFERENCES CITED

Cathles, L.M., and Shannon, R., 2007, How potassium silicate alteration suggests the formation of porphyry ore deposits begins with the nearly explosive but barren expulsion of large volumes of magmatic water: *Earth and Planetary Science Letters*, v. 262, p. 92–108, <https://doi.org/10.1016/j.epsl.2007.07.029>.

Cernuschi, F., Dilles, J.H., and Creaser, R., 2013, Hydrothermal alteration, SWIR-mineral mapping, vein distribution and age of the Haqira-East Cu-Mo porphyry, *in* Jonsson, E., et al eds., *Mineral Deposit Research for a High-Tech World, Proceedings of the 12th SGA (Society for Geology Applied to Mineral Deposits) Biennial Meeting*, Uppsala, Sweden, v. 2, p. 782–785.

Crank, J., 1975, *The Mathematics of Diffusion* (2nd edition): Oxford, UK, Clarendon Press, 414 p.

Geiger, S., Haggerty, R., Dilles, J.H., Reed, M.H., and Matthäi, S.F., 2002, The evolution of the early hydrothermal alteration at Butte, Montana: New insights from reactive transport modeling: *Geofluids*, v. 2, p. 185–201, <https://doi.org/10.1046/j.1468-8123.2002.00037.x>.

Huang, R., and Audétat, A., 2012, The titanium-in-quartz (TitaniQ) thermobarometer: A critical examination and re-calibration: *Geochimica et Cosmochimica Acta*, v. 84, p. 75–89, <https://doi.org/10.1016/j.gca.2012.01.009>.

Mercer, C.N., Reed, M.H., and Mercer, C.M., 2015, Time scales of porphyry Cu deposit formation: Insights from titanium diffusion in quartz: *Economic Geology and the Bulletin of the Society of Economic Geologists*, v. 110, p. 587–602, <https://doi.org/10.2113/econgeo.110.3.587>.

Reed, M., Rusk, B., and Palandri, J., 2013, The Butte magmatic-hydrothermal system: One fluid yields all alteration and veins: *Economic Geology and the Bulletin of the Society of Economic Geologists*, v. 108, p. 1379–1396, <https://doi.org/10.2113/econgeo.108.6.1379>.

Seedorf, E., Dilles, J.H., Proffett, J.M., Jr., Einaudi, M.T., Zurcher, L., Stavast, W.J.A., Johnson, D.A., and Barton, M.D., 2005, Porphyry deposits: Characteristics and origin of hypogene features, *in* Hedenquist, J.W., et al., eds., *Economic Geology 100th Anniversary Volume*: Littleton, Colorado, Society of Economic Geologists, p. 251–298.

Spencer, E.T., Wilkinson, J.J., Creaser, R.A., and Seguel, J., 2015, The distribution and timing of molybdenite mineralization at the El Teniente Cu-Mo porphyry deposit, Chile: *Economic Geology and the Bulletin of the Society of Economic Geologists*, v. 110, p. 387–421, <https://doi.org/10.2113/econgeo.110.2.387>.

Taylor, H.P., Jr., 1968, The oxygen isotope geochemistry of igneous rocks: Contributions to Mineralogy and Petrology, v. 19, p. 1–71, <https://doi.org/10.1007/BF00371729>.

von Quadt, A., Erni, M., Martinek, K., Moll, M., Peytcheva, I., and Heinrich, C.A., 2011, Zircon crystallization and the lifetimes of ore-forming magmatic-hydrothermal systems: *Geology*, v. 39, p. 731–734, <https://doi.org/10.1130/G31966.1>.

Watson, E.B., and Cherniak, D.J., 2015, Quantitative cooling histories from stranded diffusion profiles: Contributions to Mineralogy and Petrology, v. 169, <https://doi.org/10.1007/s00410-015-1153-4>.

Zhang, L.G., Liu, J.X., Zhou, H.B., and Chen, Z.S., 1989, Oxygen isotope fractionation in the quartz-water-salt system: *Economic Geology and the Bulletin of the Society of Economic Geologists*, v. 84, p. 1643–1650, <https://doi.org/10.2113/jgsecongeo.84.6.1643>.

Manuscript received 11 March 2018
 Revised manuscript received 20 May 2018
 Manuscript accepted 23 May 2018

Printed in USA